Optical, Structural and Morphological Study of CdS Nanoparticles: Role of Sulphur Source

M. M. Kamble, M.Sc., M.Phil., Ph.D.
PDEA'S Anantrao Pawar College, Pirangut, Mulshi, Pune, Maharashtra, India, ORCID 0000-0001-6835-5674
S. R. Rondiya, M.Sc., M.Phil, Ph.D.
School of Chemistry, Cardiff University, Cardiff, CF10 3AT, Wales, UK, ORCID 0000-0003-1350-1237
B. R. Bade, M.Sc., M. Phil.
School of Energy Studies, Savitribai Phule Pune University, Pune, Maharashtra, India, ORCID 0000-0001-8450-6807
K. B. Kore, M.Sc.
School of Energy Studies, Savitribai Phule Pune University, Pune, Maharashtra, India, ORCID number
M. P. Nasane, M.Sc.
School of Energy Studies, Savitribai Phule Pune University, Pune, Maharashtra, India, ORCID number
N. Y. Dzade, M.Sc., M.Phil, Ph.D.
The School of Chemistry, Cardiff University, Cardiff, CF10 3AT, Wales, UK, ORCID 0000-0001-7733-9473
*A. M. Funde, M.Sc., M.Phil, Ph.D.
School of Energy Studies, Savitribai Phule Pune University, Pune, Maharashtra, India, ORCID 0000-0002-6353-1103
*S. R. Jadkar, M.Sc., Ph.D.
Department of Physics, Savitribai Phule Pune University, Pune, Maharashtra, India, ORCID number
*adinathf@gmail.com (AMF), sandesh@physics.unipune.ac.in (SRJ) +91 20 25695201

Cadmium sulfide (CdS) nanoparticles were synthesized by simple and low cost homemade hot injection method at low process temperature using different sulphur sources. The effects of sulphur concentration on the structural, morphological, and optoelectronic properties of synthesized CdS films were studied using a range of characterization techniques: X-ray diffraction (XRD), Raman spectroscopy, field emission scanning electron microscopy (FESEM) and UV-Visible spectroscopy. The XRD studies revealed the formation of hexagonal type CdS nanoparticles. The varying morphology dependence on the sulphur source was ascertained from FESEM analysis. The longitudinal optical (LO) phonon vibrational modes of CdS were assigned in Raman spectra at 300 and 600 cm^{-1}. The band gap of the CdS particles was estimated to be 2.30 eV from Tauc's plots. Consistent with the experimental results, our first-principles DFT calculations predict the band gap of CdS nanoparticles to increase with decreasing S concentration: $Cd_{52}S_{52}$ (2.38 eV) $Cd_{52}S_{51}$ (2.52 eV) and $Cd_{52}S_{50}$ (2.65 eV), with both the valence and conduction band edges demonstrated to be dominated by S-p states.

Keywords: Computational Studies of CdS, CdS nanoparticles, Thin film, Optical properties, Refractive index, Energy gap, CdS for solar cell.

List of notations

$\varepsilon(\omega)$: complex dielectric function, function of frequency, ω

Γ: center of the Brillouin zone (0 0 0)

HSE06: a hybrid exchange–correlation functional used in VASP simulations

α: absorption coefficient

λ: wavelength

β: full width at half maximum (FWHM) of XRD peak

$h\upsilon$: photon energy

$d_{x\text{-ray}}$: average crystallite size estimated from x-ray diffraction analysis

ρ: relative density of CdS films

$\boldsymbol{n_f}$: refractive index of synthesized film of CdS

$\boldsymbol{n_b}$: the refractive index of bulk CdS

E_g: bandgap of material

B : Tauc's constant, a characteristic parameter of material independent of photon energy

K : extinction coefficient

1. Introduction

The photovoltaic device that converts sunlight into electricity using photovoltaic effect is an expedient and sustainable method to resolve the problems of energy demand. Nowadays commercially solar cell are fabricated using silicon wafer, which exhibit superior stability and high power conversion efficiency (PCE) of about 15–20%.[1] However, due to the high cost of such solar cells, research is being focused on new device architecture of thin film Perovskite technology. The Perovskite solar cells (PSCs) is an innovative type of photovoltaic technology which has exhibited a fast improvement in efficiency from 3.8% in 2009 to 24.2% in 2019.[2] The CdS thin films are used as an electron-transport layer instead of regular TiO_2 layer in perovskite solar cells.[3, 4] CdS is also used as a window and a hole blocking layer in CdTe based and perovskite solar cells respectively.[5] Thus, cadmium sulfide (CdS) is an attractive direct band gap semiconductor material because of several applications in photo catalysis, photonics, optoelectronics and photovoltaic devices.[6] A variety of preparation methods with different precursors of cadmium and sulphur have been used to synthesize CdS nanocrystals to obtain desired physical, structural and opto-electronic properties. These synthesis techniques include sol-gel[7], hydrothermal[8], solvothermal[9], co-precipitation[10], photochemical, polyol[11], ion implantation[12], microwave-assisted[13], electron beam evaporation[4] etc. These methods are either expensive, hazardous, moisture sensitive, extremely toxic, or energy intensive. Therefore, the fabrication of device quality CdS material with less cost and a simple approach is still a challenge for both industry and researchers. Hot injection method (HIM) is a lucrative option owing to its capability to synthesize device quality CdS nanocrystals. The hot injection method is safe, low cost, environment-friendly, and suitable for large-scale production of CdS nanocrystals with high stability. The structural, optical, morphological, and electrical properties of CdS nanocrystals can be precisely controlled by changing the synthesis parameters such as reaction time, process temperature, injection temperatures etc.

2. Experimental Section

The CdS nanocrystals have been prepared by the hot injection method (HIM) using oleylamine as solvent, surfactant and capping ligand. **Figure 1** depicts a schematic for the facile hot injection setup used for synthesis of CdS nanocrystals. Cadmium chloride monohydrate $CdCl_2.H_2O$ (0.2 M) was added to 10 ml oleylamine in 100 ml three necked flask with one end connected alternately to vacuum and argon gas container, another for sulfur solution injection and the third one for the thermocouple to measure reaction temperature. The resulting solution was stirred and heated to a constant temperature of 160 °C under vacuum and purged with Ar gas for 30 min. The Ar purging procedure was repeated 10 times to ensure complete elimination of air from the system. Once the Cd-oleylamine complex turned into a light yellow solution, the temperature was raised to 230 °C for an hour, since the crystallite size and morphology of resultant nanoparticles depend on this reaction temperature.

In the first set of experiments, the elemental sulfur powder (S1 source, 0.5 M to 2.5 M) was dissolved in 5 ml oleylamine and stirred gently with constant heating temperature of 80 °C for 45 min. The resulting sulphur solution was then injected into the Cd-oleylamine complex and the mixture solution was heated to reaction temperature of 230 °C and aged for half an hour, forming a homogeneous yellowish solution. This solution was then allowed to cool at room temperature. The whole reaction was carried out in an alternate vacuum and argon atmosphere. The same procedure was repeated for the second set of experiment in which another sulphur source (S2 source, 0.15 M to 0.35 M), 50% each of thiourea $NH_2.CS.NH_2$ and sodium sulphide flakes pract ($Na_2S.XH_2O$) was used. The CdS nanocrystals were dispersible in organic solvents such as toluene and iso-propanol, hence 5 ml of toluene and 40 ml of iso-propanol was added in order to cause the CdS nanocrystals to be precipitated. The precipitate was retrieved by centrifugation at 2500 rpm, producing colloidal yellowish CdS nanocrystals. This colloidal precipitate of CdS was then developed into a thin film on soda lime glass by using the Doctor Blade method.[14] The films were post-treated at a temperature of 50°C to dry the film. The intention to use this low temperature was to avoid energy intensive steps. The resultant CdS films were then taken out for characterization.

2.1. Characterizations:

The optical band gap, optical constants namely, refractive index, extinction coefficient and relative density of as-deposited CdS films was deduced using a UV-Visible spectrophotometer (JASCO make, V-670 model) in the wavelength range 250–800 nm. The Raman spectra of CdS films were recorded with a Horibra-JobinYvon LABRAM-HR apparatus in the range 200–1200 cm^{-1}. The spectrometer has backscattering geometry for detection of Raman spectrum with the resolution of 1 cm^{-1}. The excitation wavelength of source was 532.8 nm line of He-Ne laser. The power of the Raman laser was kept at 1 mW to avoid laser induced crystallization in the films. The low angle X-ray diffraction pattern of the CdS films was obtained by X-ray diffractometer (Bruker D8 Advance, Germany) using Cu Kα line (λ =1.54 Å) at a grazing angle of 1°. The FTIR spectra were recorded in the transmission mode by using FTIR spectrophotometer (JASCO, 6100-type A) in the range 400–4000 cm^{-1}.

2.2. Computational Details:

The electronic structure calculations were performed using the Vienna Ab initio Simulation Package (VASP), [15, 16] a periodic plane wave density functional theory (DFT). Geometry optimization was performed with the PBE functional[17] based on conjugate-gradient algorithm until the residual Hellmann–Feynman forces on all relaxed atoms reached 10^{-3} eV $Å^{-1}$. The interactions between the valence electrons and the cores were described with the projected augmented wave (PAW) method[18], which performs a fully relativistic calculation for the core-electrons and treats valence electrons in a scalar relativistic approximation.[19] The Brillouin Zone of bulk CZTS was sampled using the Γ-centered 5x5x3 k-mesh with energy cut-off of 600 eV. For accurate determination of the electronic structures, the screened hybrid functional HSE06 with 25% Hartree−Fock exchange was used.[20] The density of states (DOS) of the CdS nanoparticles was calculated using tetrahedron method with Bloch corrections.[21] The optical properties were calculated from the complex dielectric function, $\varepsilon(\omega) = \varepsilon_1(\omega) + i\ \varepsilon_2(\omega)$ within the independent-particle formalism..

3. Results and Discussion:

3.1 X-ray Diffraction Study:

The effects of sulphur concentration on the size, crystallinity and crystal phases of the CdS films were studied from X-ray diffraction (XRD) pattern. The films grown at various sulphur concentrations with S1 and S2 sources are shown in Figure 2(a) and 2(b) respectively. The XRD patterns show peak at 2θ values of 24.92°, 26.66°, 28.32°, 36.82°, 43.90°, 48.17° and 52.10° corresponding to the (100), (002), (101), (102), (110), (103) and (112) crystal orientations respectively. The XRD patterns are well matched with JCPDS #01-080-0006 of pure hexagonal CdS. As seen from **Figure 2(a) and 2(b)**, the diffraction peaks of all the samples become more intense with increasing sulphur concentrations, indicating improvement in the crystallinity. The crystallinity of CdS nanocrystals grown by hot injection method is found

to depend on i) the molar ratio of cadmium to sulphur precursor, ii) molar ratio of Cd and S precursors to oleyamine capping ligand, iii) reaction temperature and iv) reaction time.[22] When sulphur solution (80 °C) is injected into Cd-oleylamine complex (230 °C), an instantaneous formation of CdS nuclei takes place. Further heating of the CdS-complex solution at a temperature of 230 °C for half an hour resulted in the nucleation CdS nanoparticles from monodispersed, free Cd and S precursors. The slow growth at relatively high temperature of 230 °C allows the nanocrystals to anneal and to form nearly defect-free hexagonal crystal type CdS, which are identical to the bulk lattice.

The average crystalline size d_{x-ray} of CdS was calculated corresponding to the strongest peak of (002) at 26.66°(2θ) using Scherrer formula $d_{x-ray} = \frac{0.9\lambda}{\beta cos\theta}$ where, λ is the wavelength of x-rays (1.54 Å), θ is the Bragg angle and β is the line width (FWHM) in radians. As shown in figure 2(a), the average crystallite size in case of S1 source was found to vary between 21.5 nm to 34.0 nm as the sulphur molar concentration changes from 0.5M to 2.5M. As seen in figure 2(b), the crystallite size enhances from 18.3 to 37.5 nm with increasing sulphur concentration from 0.15 M to 0.25 M, further increasing S2 concentration, crystalline size decreases. Such behavior is due to the fact that initial reactants composition determines the development of the growth mechanism.[23] The formation of CdS nanocrystals using the hot injection method is demonstrated to follow the Oswald Ripening (OR) principle.[24] According to the OR principle, small solid particles dispersed in their own saturated solution, dissolved and subsequently redeposit on the larger particles in the same solutions. That means the smaller crystals acts as fuel for the growth of bigger crystals, hence the average crystalline size of the CdS nanocrystals grown by HIM is large enough in comparison to other techniques.

CdS can exist in the cubic or hexagonal structure or sometimes a mixture of both phases. The hexagonal phase has a higher optical transmission and good electrical conductivity relative to the cubic phase; the hexagonal CdS thin films are more suitable to be n-type window layer for CdTe solar cell.[25] Thus the CdS grown by HIM has advantages in the thin film solar cells.

3.2 FTIR Analysis:

The FTIR spectra of the CdS films deposited at different sulphur concentrations with S1 and S2 sulphur sources are shown in **Figure 3(a) and 3(b)** respectively. The FTIR technique is used to identify different bonding configurations present in the CdS films. As seen from the FTIT spectra 3(a) and 3(b), in the higher energy region, the absorption peaks located nearly at 3618 and 3740 cm^{-1} can be assigned to O-H stretching of adsorbed moisture on the CdS surface.[26] The strong absorption band located at ~ 670 cm^{-1} is observed in both the set which is corresponds to the Cd-S stretching vibrational mode, which confirms the formation of CdS. [27] The FTIR spectra of CdS films deposited at different S1source is shown in figure 3(a). This FTIR spectrum also exhibits a weak absorption bands centered at ~800-950 cm^{-1}, ~1200 cm^{-1} and ~1376-1460 cm^{-1}, which correspond to the C-C stretching band[28], C-CH bending[29] and sulphate S=O group, respectively.[30] The medium strong absorption bands observed at 1512 cm^{−1} can be assigned to N-H bending vibrations[31], which suggest that there are still a few oleylamine ligands bonded with CdS after the washing process. The vibrational band at ~1625 cm^{-1} is assigned to the symmetric bending of water molecule.[32] All the samples synthesized at different sulphur concentrations show the predominant vibrational peak located nearly at 1732 cm^{-1}, which corresponds to the carbonyl group (C=O).[33] As shown from figure 3(b), CdS films synthesized at different S2 source concentration shows the similar bonding configurations as that of S1 source. The detection of the C=O and N-H peaks from the FTIR analysis indicate that the oleyamine acts as both a binder and stabilizer for the synthesis of CdS.

3.3 Raman Spectroscopic Analysis:

The Raman spectra of the synthesized CdS films using S1 source are shown in **Figure 4**. The film deposited at 1 M sulphur source shows three distinct peaks with different intensities. The peaks located at 300 and 600 cm^{-1} are assigned to the longitudinal optical phonon vibrations (LO), which are in good agreement with those reported by Gilicet al.[34] at 305 and at 611 cm^{-1} for the Raman shift of bulk CdS crystal. In the present study, Raman shift of CdS film deposited at different sulphur concentration shows the shift in longitudinal optical phonon frequency from 305 cm^{-1} to 300 cm^{-1}, and 611 cm^{-1} to 600 cm^{-1}. The red shift in the LO mode of CdS thin film compared to the CdS bulk may due to phonon confinement effect, imperfections, impurity, valence band mixing and non-spherical geometry of the nanostructures. [34, 35] The Raman shift observed nearly at 391 cm^{-1} corresponds to the transverse optical phonon vibration of CdS.

3.4 Optical properties:

The UV-Vis absorption spectra of the CdS films recorded at room temperature are shown in **Figure 5 (a) and 5 (b)**. The film deposited at different S1 source concentration shows strong absorption between 300 nm to 500 nm with the absorption edge at about 500 nm, whereas the film deposited with S2 source concentration shows the absorption edge nearly at 490 nm. This suggests that the band gap energy of S2

source synthesized CdS films is larger than that those synthesized using S1 source. The optical band gap of the CdS films is calculated from the dependence of the absorption coefficient (α) on the photon energy (hυ), using the Tauc's relation (αhυ)=B(hυ-E$_g$)^n [36],where, B is the Tauc's constant, which is characteristic parameter independent of photon energy, h is the Planck's constant, υ is photon frequency, and E$_g$ is the band gap of the material. The exponent n depends on type of transition and it takes values of 1/2, 2, 3/2 and 3 corresponding to allowed direct, allowed indirect, forbidden direct and forbidden indirect transitions, respectively. As Cadmium sulphate has direct allowed transitions we choose n = 1/2. The optical band energy of CdS films was determined by extrapolating the straight line portion of the graph plotted (αhυ)^2 against energy (hυ). The intercept of the extrapolated line on the energy (hυ) axis give the band gap value of the material. The band gap of the film deposited using the S1 and S2 source concentration are estimated at 2.20 and 2.30 eV, respectively as shown in **Figure 6 (a) and 6(b)** respectively. The small difference in the band gap values may be attributed to the change in the crystallite sizes as reported in XRD analysis section.[37] The band gap of the CdS films deposited at different sulphur concentration with S1 and S2sulphur sources shows the red shift in the bandgap in comparison with bulk CdS (2.42 eV). The refractive index of the CdS films deposited at different S1 and S2 source was calculated using Herve-Vandamme formula.

$n = \sqrt{1 + \left(\frac{P}{E_g + Q}\right)}$ where, P (=13.6 eV) and Q (=3.4 eV) are constants.

Refractive index gives the information about vacancies present in the deposited film and define the measurement of density i.e. decrease in refractive index means decrease the material density in the film.[38, 39] Refractive index of the films deposited at different S1 source is found in the range of 2.57 to 2.62. The maximum refractive index 2.63 was calculated corresponds to the 0.25 molar S2 source concentrations. Relative density (ρ) of CdS films is calculated from The Lorentz-Lorentz relation[5]

$$\rho = \left(\frac{n_f{}^2 - 1}{n_f{}^2 + 1}\right)\left(\frac{n_b{}^2 + 1}{n_b{}^2 - 1}\right)$$

Where, n_f and n_b be the refractive index of synthesized CdS film and bulk CdS respectively (n_b=2.529). The calculated values of ρ are 1.0101, 1.0197, and 1.0220 for the films synthesized at 0.5, 1.0 and 1.5 molar of S1 source and 1.0126, 1.0243, 1.0101 and 1.0077 for the films fabricated at 02, 0.25, 0.30, and 0.35 molar of S2 source respectively.

The extinction coefficient (K) was evaluated by a standard relation $K = (\alpha * \lambda)/4\Pi$.[40] The K gives information about material related to absorbance of incident light. As seen from **Figure 7(a) and 7(b)** extinction coefficient increases with photon energy and found maximum nearly at 2.5 eV for S1 and S2 source after that K decreases. It can also be seen that the extinction coefficient is maximum at 0.5M of S1 source and 0.25 M of S2 source.

3.5 Density Functional Theory (DFT):

Further insights into the structure, electronic and optical properties of the CdS nanoparticles were gained from first-principles DFT calculations. We have considered a spherical structure of the hexagonal nanoparticle of composition: Cd$_{52}$S$_{52}$, Cd$_{52}$S$_{51}$, and Cd$_{52}$S$_{50}$in order to investigate the effect of sulphur concentration on the predicted electronic and optical properties. The Cd$_{52}$S$_{51}$, and Cd$_{52}$S$_{50}$ compositions were created by removing one and two S atoms (vacancies), respectively from the Cd$_{52}$S$_{52}$ composition. The optimized structures of the CdS nanoparticles with varying S concentration are shown in **Figure 8 (a-c)**. The average Cd–S bond distance in the Cd$_{52}$S$_{52}$ composition is predicted at 2.532 Å. We observer small local distortion in the Cd$_{52}$S$_{51}$, and Cd$_{52}$S$_{50}$ due the creation of S vacancies, which resulted in the elongation of the Cd–S bond distances (2.696 Å) in the vicinity of the S vacancies compared to those far away from the S vacancy sites (2.532 Å). Shown in Figure 8 (d-f) are the corresponding electronic structures of the Cd$_{52}$S$_{52}$, Cd$_{52}$S$_{51}$, and Cd$_{52}$S$_{50}$ nanoparticles. An analysis of the projected density of states in the valence and conduction band edges of the CdS nanoparticles are composed mainly of the S-p states. Compared the 1:1 ratio Cd$_{52}$S$_{52}$ composition, we observe gap stated in the Cd$_{52}$S$_{51}$, and Cd$_{52}$S$_{50}$, which can be attributed to the presence of S vacancy defects. The band gap of the Cd$_{52}$S$_{52}$, Cd$_{52}$S$_{51}$, and Cd$_{52}$S$_{50}$ nanoparticles is predicted at 2.38, 2.52, 2.65 eV, respectively, indicating the band gap increases with decreasing S concentration.

To gain further insight into the optical properties of the CdS nanoparticles with decreasing S content, the frequency-dependent dielectric function $\varepsilon(\omega) = \varepsilon_1(\omega) + i\varepsilon_2(\omega)$ at energy has been computed. The optical properties of semiconducting materials are inherently linked to their electronic properties, hence the predicted differences in the electronic band gaps is expected to dictate the optical properties of the CdS nanoparticles. The calculated real (dispersive, ε_1) and imaginary (absorptive, ε_2) parts of the dielectric function for CdS nanoparticles are shown in **Figure 9 (a-c)**. From the real part of the dielectric function, the dielectric constants of the areCd$_{52}$S$_{52}$, Cd$_{52}$S$_{51}$, and Cd$_{52}$S$_{50}$ nanoparticles are calculated at 9.48, 7.19, and 6.17, respectively. The absorbance of Cd$_{52}$S$_{52}$, Cd$_{52}$S$_{51}$, and Cd$_{52}$S$_{50}$ nanoparticles (Figure 9d) starts just after 2 eV, which close to their fundamental band gaps, but in general a higher absorbance is predicted for the Cd$_{52}$S$_{52}$ nanoparticle in the visible light region, which is consistent with its smaller band gap than that of the Cd$_{52}$S$_{51}$, and Cd$_{52}$S$_{50}$ nanoparticles.

We also a higher reflectivity in the $Cd_{52}S_{52}$ nanoparticle (25%) than for the $Cd_{52}S_{51}$ (19%), and $Cd_{52}S_{50}$ (18%) nanoparticles (Figure 9e). A higher refractive index is also predicted for the $Cd_{52}S_{52}$ nanoparticle (3.01) than for the $Cd_{52}S_{51}$ (2.56), and $Cd_{52}S_{50}$ (2.45) nanoparticles (Figure 9f).

3.6 FESEM Analysis:

Figure10 (a) is the FE-SEM Image of CdS films synthesized using 2.5 MS1 Source concentration and (b) is the FE-SEM Image of CdS films synthesized using 0.35 M S2 Source concentration. The CdS film deposited at 2.5 M sulphur source (S1) reveal highly agglomerated, densely packed, smooth, uniform and spherical shaped nanoparticles Figure 10 (a). Vertically oriented rod like structures Figure 10 (b) were obtained due to larger grains are formed by the combination of smaller grains revealed to the increment in the diffusion length of the charge carriers and provides a conducting link when the CdS film is deposited using Thiourea and Sodium sulphide Flakes Pract as a sulfur source (S2).[41] It can thus be concluded from the FESEM analysis that the morphology of CdS films can be tuned by sulphur source.

Conclusion

High-quality CdS nanoparticle films have been successfully synthesized using hot injection method and deposited on soda lime glass substrate using doctor blade method. The influence of sulphur concentration with S1 and S2 sulphur sources on the structural, morphological, and optoelectronic properties of the CdS films has been investigated in detail. Formation of hexagonal CdS is confirmed by XRD, FTIR and Raman analysis. The maximum crystallite size of CdS was found to be 37.5 nm in case of S2 source with 0.25 M sulphur concentration. The UV–VIS spectroscopic analysis shows the CdS films exhibit a red shift in absorption edge compared with bulk CdS. Maximum refractive index 2.63 observed corresponding to the 0.25 molar concentration for S2 source. The FESEM studies show the morphology of the CdS is sulphur source dependent. First-principles DFT calculations predict the band gaps of CdS nanoparticles to increase with decreasing S concentration: $Cd_{52}S_{52}$ (2.38 eV) $Cd_{52}S_{51}$ (2.52 eV) and $Cd_{52}S_{50}$ (2.65 eV) and the differences in the electronic properties is shown to influence the optical properties of the CdS nanoparticles. The morphology controlled synthesis of CdS thin films using S1 and S2 sulphur sources provide a promising approach for synthesis of CdS nanoparticles with tailored morphology and optoelectronic properties. Thus from present study we conclude that CdS thin film synthesized was more suitable for n-type window layer for CdTe solar cell and electron-transport layer in perovskite solar cells.

References
1. Guerrero-Lemus, Ricardo, Shephard, Les E (2017) Low-Carbon Energy in Africa and Latin America: Renewable Technologies, Natural Gas and Nuclear Energy, *Springer International Publishing* pp. 149–173.
2. NREL, Best Research-Cell Efficiencies, https://www.nrel. gov/pv/assets/pdfs/best-research-cell-efficiencies-190416.pdf.
3. Anuradha Purohit, S. Chander and M.S. Dhaka (2018) Thermal evolution of physical properties of evaporated CdS thin films for perovskite solar cell applications. *Vacuum* **153**: 35-38.
4. Subhash Chander and Dhaka M. S. (2017) Optimization of substrates and physical properties of CdS thin films for perovskite solar cell applications. *J. Mater. Sci: Mater. Electron.* **28**: 6852-6859.
5. Subhash Chander and Dhaka M. S. (2017) Optical and structural constants of CdS thin films grown by electron beam vacuum evaporation for solar cells. *Thin Solid Films* **638:** 179 -188.
6. Qutub N and Sabir S (2012) Optical, thermal and structural properties of CdS quantum dots synthesized by a simple chemical route. *International Journal of Nanoscience and Nanotechnology* **8**: 111–120.

7. Zhang H (2016) Effects of post-annealing treatment on the structure and photoluminescence properties of CdS/PS nanocomposites prepared by sol-gel method. Optoelectronic *Letters* **12**: 81–84.

8. Chen R, Han B, Yang L et al. (.2016) Controllable synthesis and characterization of CdS quantum dots by a microemulsion-mediated hydrothermal method. *Journal of Luminescence* **172**: 197–200.

9. Ren B, Cao M, Zhang Q et al. (2016) Controllable synthesis of CdS nanowire by a facile solvo thermal method and its temperature dependent photoluminescent property. *Journal of alloys and compounds* **659**:74–81.

10. Elavarthi P, Kumar A A, Murali G et al. (2016) Room temperature ferromagnetism and white light emissiveCdS:Cr nanoparticles synthesized by chemical co-precipitation method. *Journal of alloys and compounds* **656**: 510–517.

11. Darwish M, Mohammadi A, Assi N (2016) Microwave-assisted polyol synthesis and characterization of pvp-capped CdS nanoparticles for the photocatalytic degradation of tartrazine. *Materials Research Bulletin* **74**: 387–396.

12. Denisca U V, Gamulin O, Tonej A et al. (2001) CdS nanocrystals formed in SiO_2 substrates by ion implantation. *Materials Science and Engineering C* **15**:105-107.

13. Yang H, Huang C, Li X et al. (2005) Luminescent and photocatalytic properties of cadmium sulfide nanoparticles synthesized via microwave irradiation. *Materials Chemistry and Physics* **90**:155–158.

14. Miskin C K, Yang W. C, Hages C J et al. (2015). 9.0% efficient $Cu_2ZnSn(S,Se)_4$ solar cells from selenized nanoparticle inks. *Progress in Photovoltaics: Research and applications* **23(5)**: 654-659.

15. Kresse G and Joubert D (1999) From ultrasoft pseudopotentials to the projector augmented-wave method. *Physical Review B.* **59 (3)**: 1758-1775.

16. Kresse G and Furthmüller J (1996) Efficiency of ab-initio total energy calculations for metals and semiconductors using a plane-wave basis set. *Computational Materials Science* **6**: 15-50.

17. Perdew J P, Burke K and Ernzerhof M (1997) Generalized Gradient Approximation Made Simple. *Physical review Letters* **78**: 1396-1399.

18. Blöchl P. E. (1994) Projector augmented-wave method. *Physical Review B.* **50 (24)**: 17953-17997.

19. Koelling D. D. and Harmon, B. N. (1977) A technique for relativistic spin-polarized calculations. *J. Phys. C* **10**: 3107

20. Krukau A V, Vydrov O A, Izmaylov A. F et al. (2006) Influence of the exchange screening parameter on the performance of screened hybrid functionals. *Journal of Chemical Physics* **125 (22)**: 224106-1-224106-5.

21. Blöchl P E, Jepsen O and Andersen O K (1994) Improved tetrahedron method for Brillouin-zone integrations. *Physical Review B.* **49** : 16223–16233.

22. Peng Z. A., and Peng X (2002) Nearly Monodisperse and Shape-Controlled CdSe Nanocrystals via Alternative Routes: Nucleation and Growth. *Journal of the American Chemical Society* **124**: 3343-3353.

23. Nieto-Zepeda K.E., Guillen-Cervantes and driguez-Rosales et al. (2017) Effect of the sulfur and fluorine concentration on physical properties of CdS films grown by chemical bath deposition. *Results in Physics* **7**: 1971-1975

24. Ghorpade U, Suryawanshi M, Shin S W et al. (2014) Towards environmentally benign approaches for the synthesis of CZTSSe nanocrystals by a hot injection method: a status review. *Chemical Communications.* **50**:11258—11273

25. Chin-Yu Y E H, Lu Z W and Froyen S (1992) Zinc-blende–wurtzitepolytypism in semiconductors. *Physical Review B.* **46**:10086–10097

26. Verma A K, Chandra P, Srivastava A et al. (2017) Optoelectronic Studies of Commercially and Lab Prepared Cadmium sulfide Chalcogenide. *Research & Reviews: Journal of Material Sciences* **5(2)**: 28–34.

27. Delacruz Terrazas E C, Ambrosio R C, Mota González M L et al. (2015)A simple method for the synthesis of CdS nanoparticles using a novel surfactant. *Chalcogenide Letters* **12(4)**: 147 – 153.

28. Feroz A M, Chattarjeeb I, Darc A A et al. (2015).Preparation and characterizations of cadmium sulfide nanoparticles. *Optik* **126**: 1240–1244.

29. Krylova V and Dukstiene N (2019) The structure of PA-Se-S-Cd composite materials probed with FTIR spectroscopy. *Applied Surface Science* **470**: 462–471.

30. Sabah A, Siddiqi S A and Salamat A (2010) Fabrication and Characterization of CdS Nanoparticles Annealed by using Different Radiations. *International Scholarly and Scientific Research & Innovation,* **4(9)**: 532-53.

31. Li Y and Yang G (2004) Studies on molecular composites of polyamide 6/polyamide 66, *Macromolecular Rapid Communications* **25 (19)**: 1714–1718.

32. Thirumala Rao G, Babu B and Joyce S R. (2015) Synthesis and characterization of VO^{2+} doped ZnO–CdS composite nanopowder. *Journal of Molecular Structure* **1081**:254-259

33. Yunfeng S, lanbo L, chunlai T et al.(2011) Facile Preparation of CdS Quantum Dots Using Hyperbranched Poly(amidoamine)s with Hydrophobic End-Groups as Nanoreactors. *Journal of Applied Polymer Science* **122(2)**:1077 – 1083.

34. Gilic M, Trajic J, Romevic N et al. (2013) Optical properties of CdS thin films. *Optical Material* **35**: 1112–1117

35. Owens F.J. and Poole C.P. (2007) Introduction to Nanotechnology, *John Wiley & Sons, Inc, Hoboken, New Jersey*, USA

36. Tauc J, in: F. Abeles (Ed.). (1972) Optical Properties of Solids. *North Holland Publications, Amsterdam*, 1034

37. Rodríguez-Rosales K, Quiñones-Galván J G, Guillén-Cervantes A et al. (2017) Nanocrystalline-CdS thin films grown on flexible PET-substrates by chemical bath deposition, *Materials Research Express.* 4(7): 075904. doi:10.1088/2053-1591/aa7858

38. Subhash Chander, A. Purohit, C. Lal and M. S. Dhaka (2017) Enhancement of optical and structural properties of vacuum evaporated CdTe Thin films. *Mater. Chem. Phys.* **185**: 202-209

39. Chander Subhash and Dhaka M.S. (2017) Thermal annealing induced physical properties of electron beam vacuum evaporated CdZnTe. *Thin Solid Films* **625**: 131-137.

40. Kariper A., Guneri E., Gode F., Gumus C., Ozpozan T (2011) The structural, electrical and optical properties of CdS thin films as a function of Ph. *Mater. Chem. Phys.* **129**:183-188.

41. Chander Subhash and Dhaka M.S. (2018) CdCl$_2$ treatment concentration evolution of physical properties correlation with surface morphology of CdTe thin films for solar cells. *Mater. Res. Bull.* **97**: 128-135.

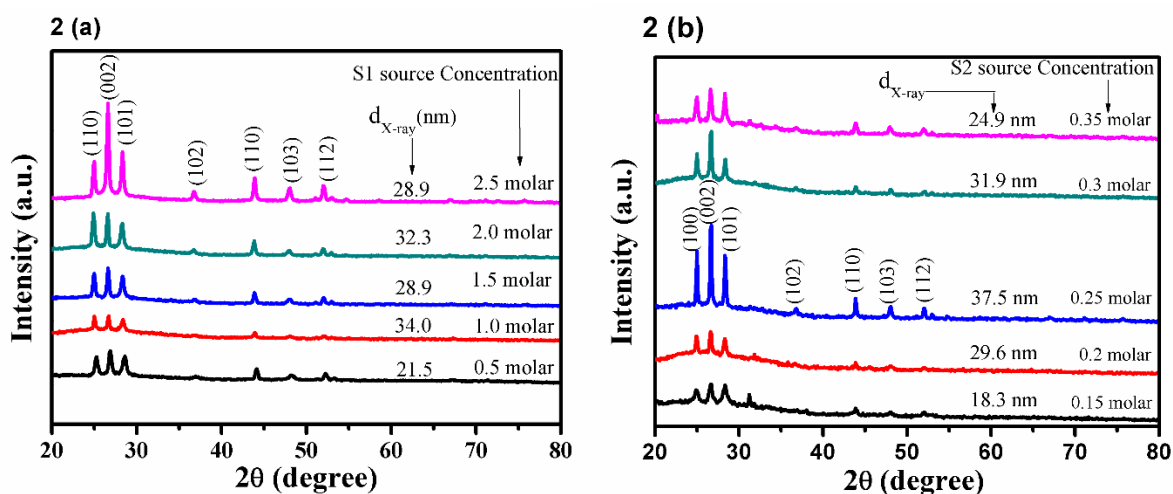**Figure 1.** Schematic of Hot Injection technique experimental setup

Figure 2. (a) XRD patterns of the CdS films synthesized at different S1 source concentration (b) XRD patterns of the CdS films synthesized at different S2 source concentration
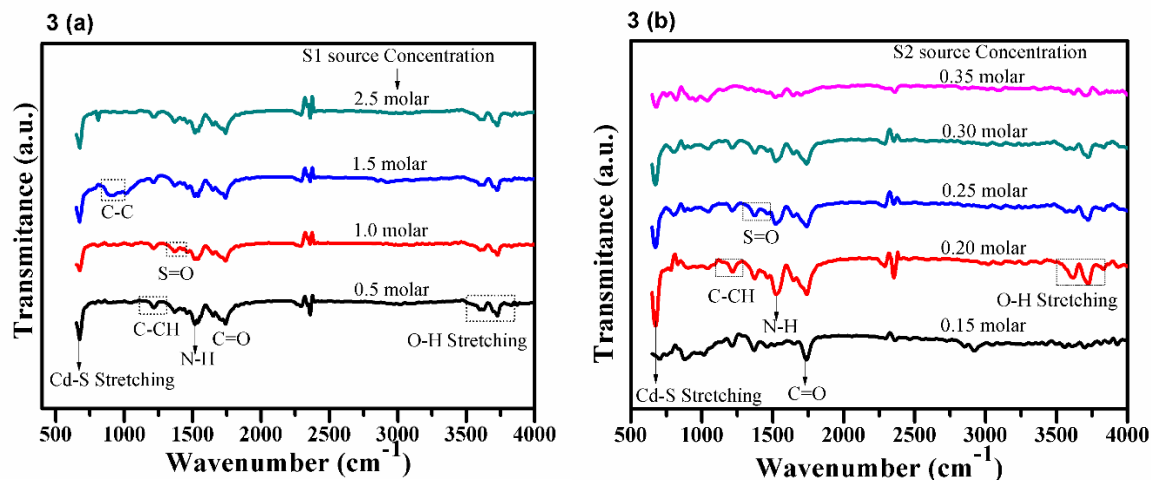
Figure 3. (a) FT-IR spectra of CdS films synthesized at different S1 source concentration, (b) FT-IR spectra of CdS films synthesized at different S2 source concentration
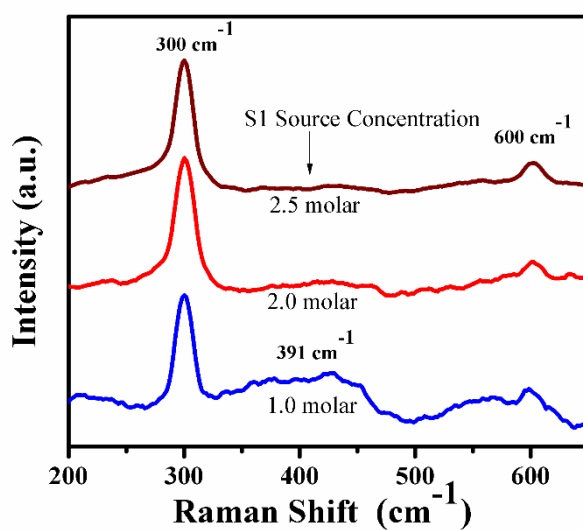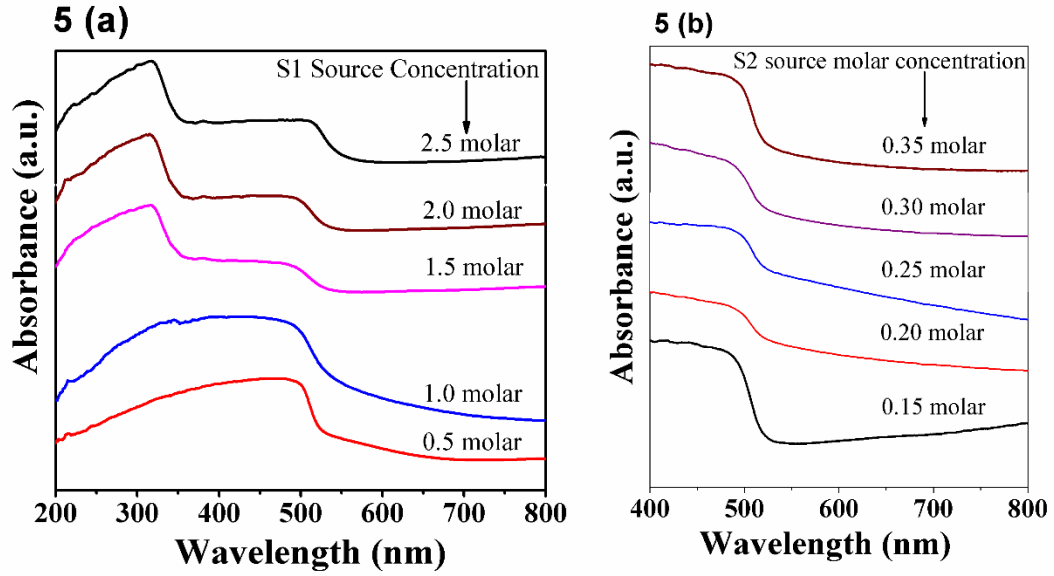

Figure 4. Raman spectra of the CdS films synthesized at various S1 source concentration

Figure 5. (a) Absorption spectra of CdS films synthesized at various S1 source concentration, (b) Absorption spectra of CdS films synthesized at different S2 source concentrations.
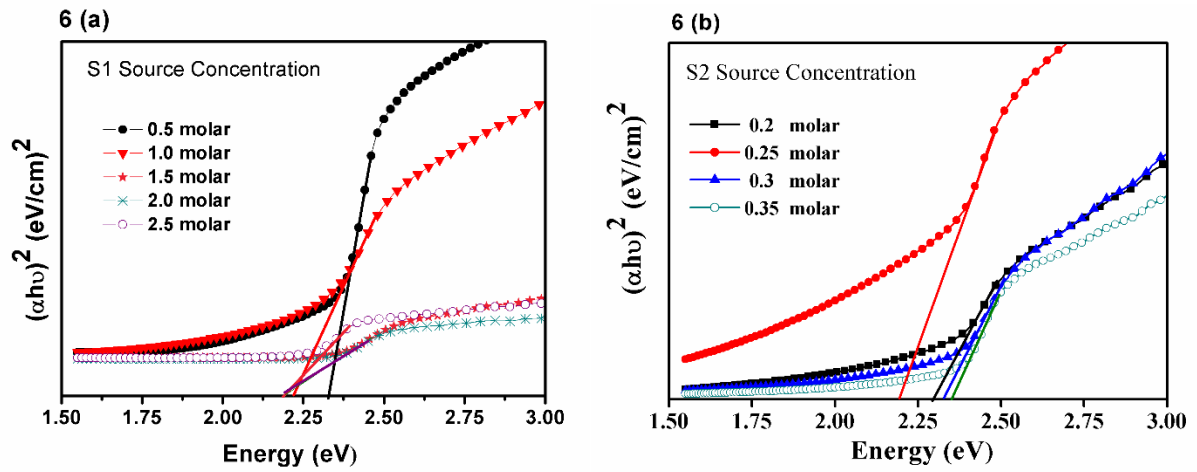

Figure 6. (a) The Tauc's Plots of CdS films synthesized at different S1 source concentrations, (b)TheTauc's Plot of CdS films synthesized at different S2 source concentrations
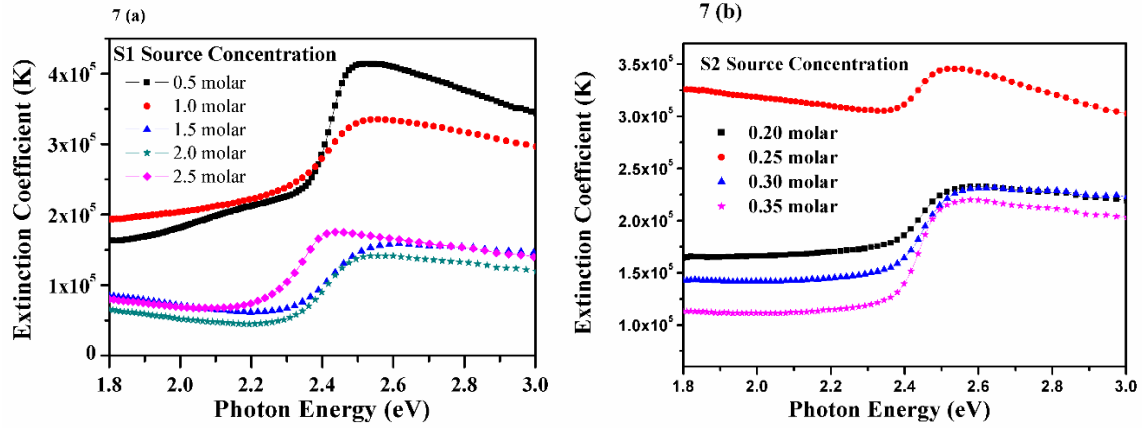
Figure 7. (a) Plot of extinction coefficient as a function of photon energy for CdS films at different S1 source concentrations, (b) Plot of extinction coefficient as a function of photon energy for CdS films at different S2 source concentrations.
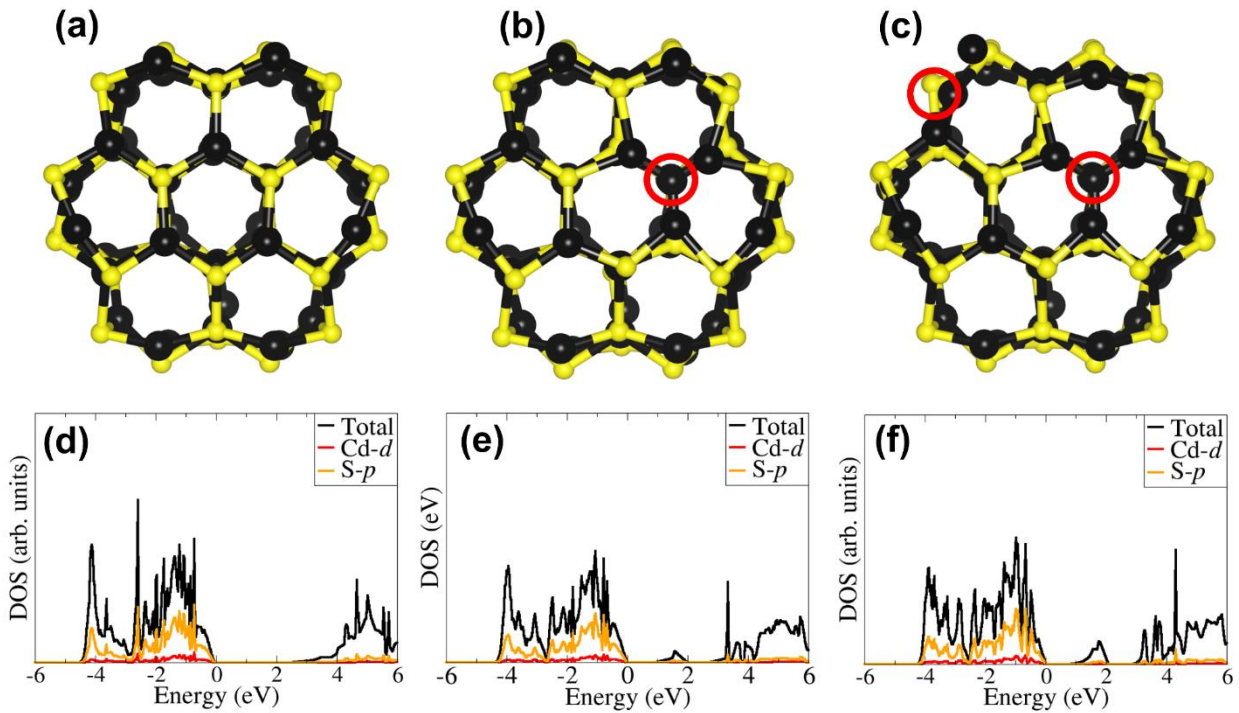

Figure 8. The optimized structures of the CdS nanoparticles with varying S concentration: (a) $Cd_{52}S_{52}$, (b) $Cd_{52}S_{51}$, and (c) $Cd_{52}S_{50}$. The S-vacancy sites are denoted by the red circles. The corresponding density of states projected on the Cd-d and S-p states are shown in (d-f). Colour scheme: Cd (black) and S (yellow).
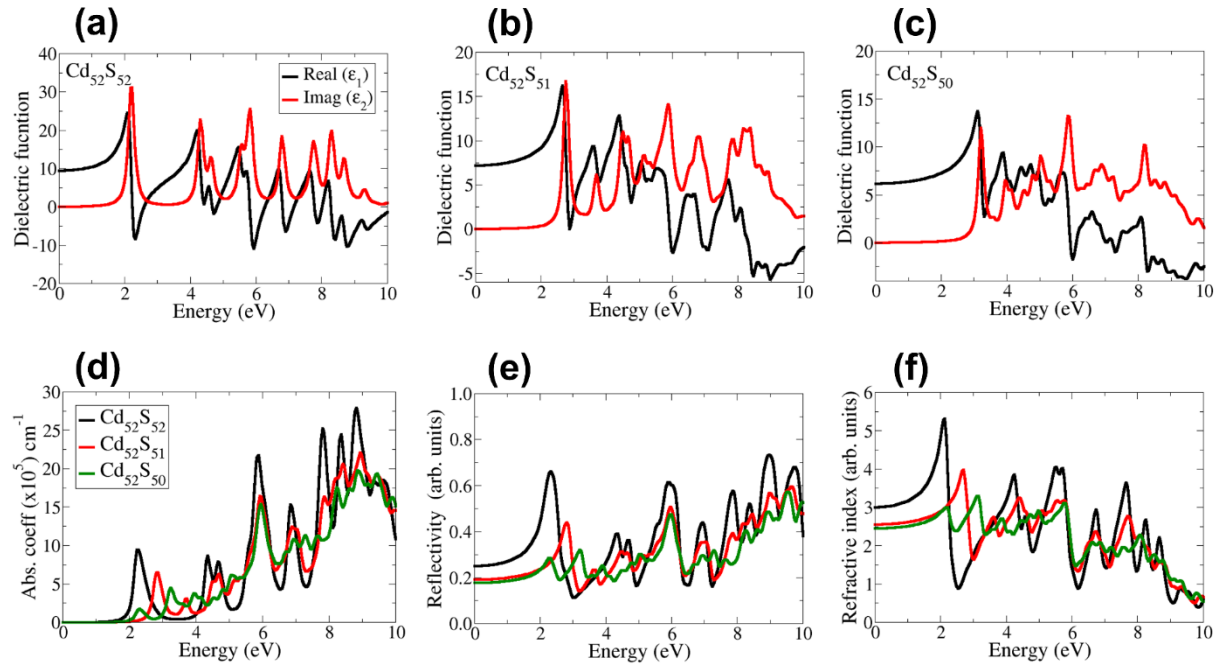
Figure 9. Calculated dielectric function (a-c) of $Cd_{52}S_{52}$, $Cd_{52}S_{51}$, and $Cd_{52}S_{50}$ nanoparticles and corresponding absorbance (d) reflectivity (e) and (d) refractive index (f).
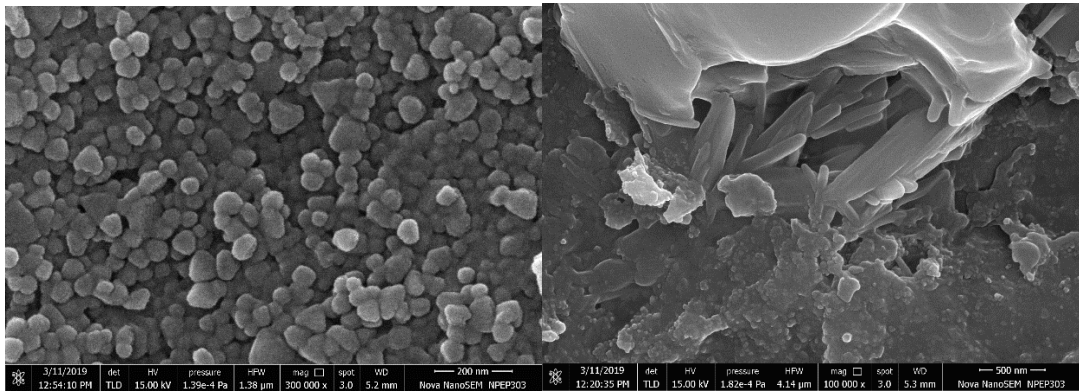

Figure 10. (a) The FE-SEM Image of CdS films synthesized using 2.5 M S1 Source concentration, (b) The FE-SEM Image of CdS films synthesized using 0.35 M S2 Source concentration